G3, 2023, 13(3), jkac338
https://doi.org/10.1093/g3journal/jkac338
Advance Access Publication Date: 27 December 2022
Neurogenetics

Function of cell adhesion molecules in differentiation of ray sensory neurons in *C. elegans*

Naoko Sakai [1,2], Peter Sun,[1] Byunghyuk Kim [1,3], Scott W. Emmons[1,*]

[1]Department of Genetics, Albert Einstein College of Medicine, Bronx, New York 162-8666, USA
[2]Department of Physiology, Tokyo Women's Medical University School of Medicine, Shinjyuku, Tokyo 10326, Japan
[3]Department of Life Science, Dongguk University, Bronx 10461, South Korea

*Corresponding author: Albert Einstein College of Medicine, Department of Genetics, 1300 Morris Park Avenue, Bronx, NY 10461, USA.
Email: scott.emmons@einsteinmed.edu

For proper functioning of the nervous system, it is crucial that neurons find their appropriate partners and build the correct neural connection patterns. Although cell adhesion molecules (CAMs) have been studied for many years as essential players in neural connections, we have yet to unravel the code by which CAMs encode synaptic specificity. We analyzed the effects of mutations in CAM genes on the morphology and synapses of a set of sensory neurons in the *Caenorhabditis elegans* male tail. B-type ray sensory neurons express 10 genes encoding CAMs. We examined the effect on axon trajectory and localization of pre-synaptic components in viable mutants of nine of these. We found axon trajectory defects in mutants of UNC-40/DCC, SAX-3/ROBO, and FMI-1/Flamingo/Celsr1. None of the mutations caused loss of pre-synaptic components in axons, and in several the level even appeared to increase, suggesting possible accumulation of pre-synapses. B-type sensory neurons fasciculate with a second type of ray sensory neuron, the A-type, in axon commissures. We found a CAM expressed in A-type functions additively with a CAM expressed in B-type in axon guidance, and lack of a CAM expressed in B-type affected A-type axon guidance. Overall, single and multiple mutants of CAM genes had limited effects on ray neuron trajectories and accumulation of synaptic components.

Keywords: *Caenorhabditis elegans*, cell adhesion molecules, neuron, development

Introduction

Since the proposal that the pattern of neural connections is controlled by individual identification tags on the cell surfaces of neurons (Sperry 1963), a number of cell adhesion molecules (CAMs) that regulate axon outgrowth and synapse formation have been identified through forward genetic and other methods (Hedgecock *et al.* 1990; Zallen *et al.* 1998; Yamagata *et al.* 2002; Shen and Bargmann 2003; Salzberg *et al.* 2013; Carrillo *et al.* 2015; Kurshan *et al.* 2018; Philbrook *et al.* 2018; Südhof, 2018; Kurshan and Shen 2019; Taylor *et al.* 2021). Despite efforts in the last few decades, we have yet to break the code by which CAMs help neurons find their appropriate partners. This is due in part to the redundant and pleiotropic functions of CAMs. There is limited information on expression patterns of CAMs in circuits of known connectivity, which has limited us in studying these parallel functions.

The nematode *Caenorhabditis elegans* has been a well-studied model organism for neuronal development because of its invariant developmental pattern and fully reconstructed neural and synaptic connectivity (White *et al.* 1986; Cook *et al.* 2019). Because of this feature, *C. elegans* has played an important role in studies of the relationship between CAMs and development (Yamagata *et al.* 2002; Shen *et al.* 2004; Salzberg *et al.* 2013; Kim and Emmons 2017; Shah *et al.* 2017; Lázaro-Peña *et al.* 2018; Philbrook *et al.* 2018; Taylor *et al.* 2021) In this study, we focused on a set of male-specific sensory neurons to investigate the relationship between CAMs, neurite trajectory, and synapse formation.

The *C. elegans* male has a set of nine bilateral pairs of sensory structures known as rays projecting from the tail embedded within a cuticular fan (Fig. 1a). Each ray has a similar structure consisting of the sensory endings of two sensory neurons of two types designated A-type and B-type (Sulston *et al.* 1980). In addition, each of the nine ray pairs has a distinct identity affecting the neurotransmitters, synaptic targets, and functions of the constituent neurons (Baird *et al.* 1991; Chow and Emmons 1994; Lints *et al.* 2004). As part of a large cohort of male-specific neurons and muscles, the ray sensory neurons are born during the L3 larval stage and differentiate through the L4 and into young adulthood (Sulston *et al.* 1980). Their cell bodies are located in a pair of bilateral lumbar ganglia. To reach their synaptic targets, ray neurons extend axons through circumferential commissures and into the pre-anal ganglion, where their growing processes branch considerably and synapse onto a number of post-synaptic targets (Fig. 1a and b). In this study, we focus on the role of CAMs in determining the trajectories and synapse formation of the B-type ray neurons (RnB, $n = 1–9$, designating the nine rays).

We have determined the expression patterns of the cell adhesion genes encoded in the *C. elegans* genome across the *C. elegans* posterior nervous system (in preparation). In our dataset, the B-type ray neurons collectively express 10 different CAMs, while the A-types altogether express 21 (Fig. 1c). The pattern is left/right

Received: November 01, 2022. Accepted: November 29, 2022

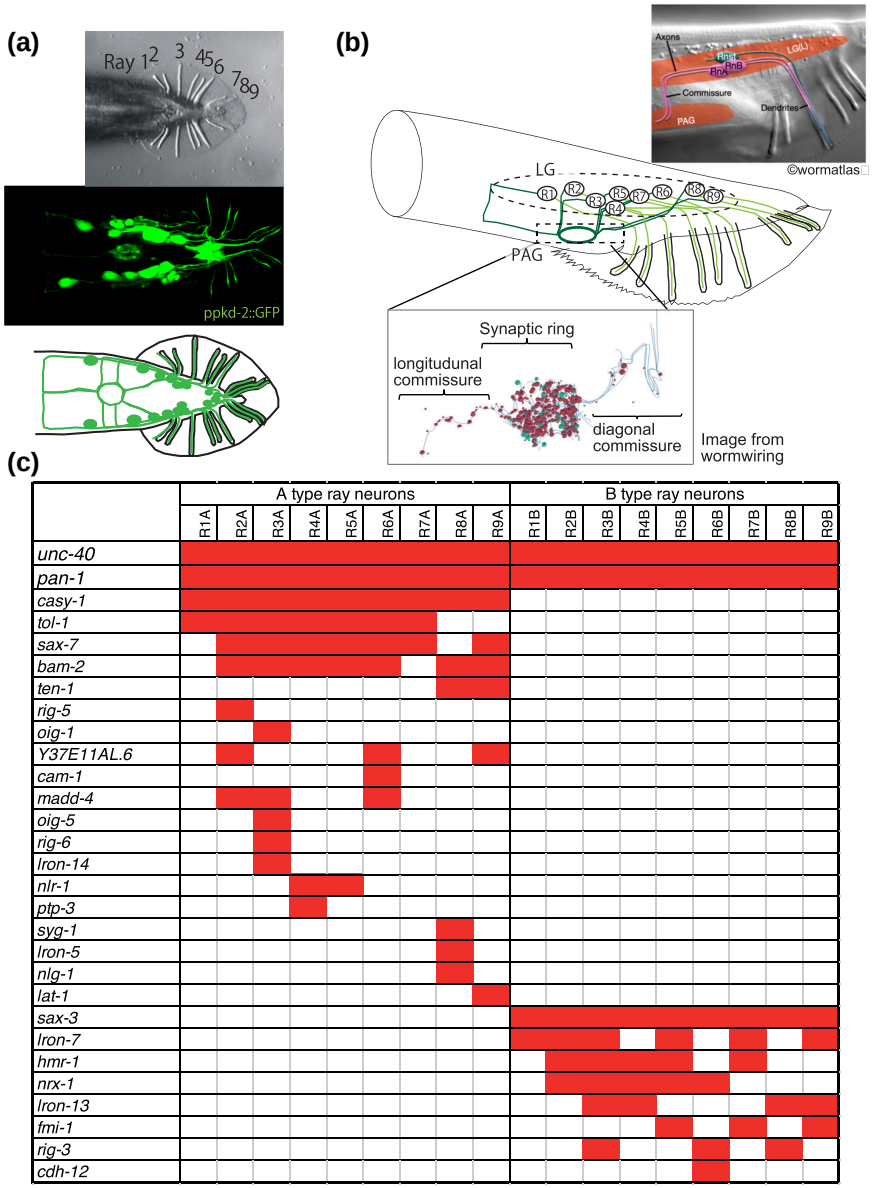

Fig. 1. CAMs expressing in ray neurons. a) A Nomarski image of the ventral view of the male tail (top), a fluorescent image of RnB neuron processes marked by pkd-2^{prom}::GFP (middle), and a schematic image of a male ray structure and RnB processes (bottom). b) Schematic image of a lateral view of the male tail (middle), schematic to explain distribution of RnA, RnB, and RnSt (ray structure cells) (top), and lateral view of the processes of R1-R9BL, as well as pre-synapses (red spheres) and gap junctions (green spheres) constructed from Electron Microscope (EM) images (https://www.wormwiring.org/). Each sphere size represents the number of EM sections containing each synapse. (bottom). The broken circle marks LG (lumber ganglion) where the cell bodies of ray neurons are located, and the broken square marks PAG (pre-anal ganglion) where the ray neurons make many synaptic connections to other neurons. Dendritic regions are shown in light lines and axonal regions are shown in dark lines. c) Expression of transcriptional reporters for CAMs in the RnA and RnB neurons. One hundred CAM genes have been examined and the genes having expression in the ray neurons are shown as red boxes.

symmetric—in each case, the left/right homologous neurons had the same expression, and it is ray and neuron-type specific—only two of the genes, *unc-40* and *pan-1*, are expressed in both A and B types. In this study, we examined the effects of mutations in the B-type-expressed genes as well as several of the A-type-expressed genes on the ray B-type axon trajectories and synapse formation, using reporters that allow us to simultaneously score both the neurite trajectory and the localization of pre-synaptic components. In a previous forward genetic screen, it was found that mutations in *unc-40/DCC* and *sax-3/ROBO* prevented the outgrowth of the B-type axons through the circumferential commissures (Jia and Emmons 2006). In a second study, B-type neuron synapse formation was affected by mutations in CAMs neurexin and neuroligin as well as by mutation in a modification enzyme that affects the sulfation pattern of sugar residues on the matrix protein glypican (Lázaro-Peña *et al.* 2018). In this study, we demonstrated the effects of mutations in *fmi-1*/flamingo and *sax-7*/L1CAM on B-type neuron trajectory. As *sax-7* is expressed in A-type but not in B-type neurons, the *sax-7* result indicates that *sax-7* functions in A-type to affect B-type neuron morphology. Overall, however, in our nearly complete survey, we found limited effects of both single and multiple mutations in most of the expressed CAM genes, suggesting the robustness of the mechanisms underlying neuronal development.

Materials and methods

Animal maintenance

All animals were maintained using standard methods (Brenner 1974). Briefly, all animals were grown on NGM plates seeded with *Escherichia Coli* OP50 at 20°C. All strains contain the *him-5(e1490)* mutation to increase the male population in selfing worms (Broverman and Meneely 1994) unless otherwise specified. For all strain information, see the Supplementary file.

Statistical analyses

All data were analyzed by Fisher's exact test or multiple comparison test using Graph-pad Prism 9.0 statistical software (RRID: SCR_002798).

Plasmid constructions and germline transformation

Plasmid constructs were generated using the In-Fusion HD Cloning Kit (Takara-bio). To construct pkd-2prom::3xnovoGFP-CLA-1, we amplified pkd-2 promoter with the primers as listed and fused into PK085 plasmid (unc-129^{prom}::3xnovoGFP-CLA1, kindly provided by P. Kurshan) digested with xbaI and sphI sites.

Pkd2_R(xbaI)	ccggggatccTCTAGATCCTCACTGACCATAGAATGG
pkd2_F(sphI)	attacgccaagcttGCATGCTAAATTCGGACTAAACATAATTATAAACATTTTGAAACATTATTA

Germ-line transformation was performed using standard microinjection techniques (Mello *et al.* 1991). Pkd-2prom::3xnovoGFP-CLA-1, pkd-2prom::BFP, pCFJ90, and PPD49.26 were co-injected into the germline.

Reporter genes used in this study

Two integrated transgenes were used to visualize the trajectories and synapses of ray B-type sensory neurons (Fig. 2a). Both utilized the promoter of the polycystin-homolog gene *pkd-2* (Barr and Sternberg 1999) to drive expression of fluorescent markers in the RnB neurons. In addition to the RnB's, this promoter drives expression in tail sensory neuron HOB and four CEM sensory neurons in the male head (Barr and Sternberg 1999).

For visualization of neuron trajectories, both transgenes included Ppkd-2 driving a cytoplasmic marker. One transgene, *bxIs30II* (strain EM1554), expressed cytoplasmic GFP along with mCherry-labeled Rab-3, the *C. elegans* homolog of mammalian Rab3, a component of synaptic vesicles (Nonet *et al.* 1997; Lázaro-Peña *et al.* 2018). The second, *bxIs33I* (strain EM1890), included cytoplasmic BFP along with RAB-3-mCherry and 3xnovoGFP-CLA1. CLA-1 is a piccolo/bassoon-like scaffolding protein active zone component (Xuan *et al.* 2017). Both strains carried a mutation in the *him*-5 gene, resulting in the presence of males in selfing hermaphrodite populations.

Microscopy and image analysis

Animals were anesthetized with 20 mM levamisole and mounted on their back on 5% agar pads on glass slides. We used 1-day-old males to observe RnB axon morphology. To observe anterior-posterior and circumferential axons, animals were observed with fluorescence microscopy (Zeiss Axio Imager A1) with 100× magnification. To observe diagonal commissures, we utilized Nikon CSU-W1spinning disk confocal microscopy with 100× magnification.

RnB synapse imaging

To visualize the pre-synaptic pattern of RnB neurons, we utilized EM1554 bxIs30[pkd-2^{prom}::gfp; pkd-2^{prom}::RAB-3-Mcherry; ttx-3p::GFP] II; him-5(e1490)V and EM1890 bxIs33[pkd-2^{prom}::3xnovoGFP-CLA1, pkd-2p::RAB-3-Mcherry, pkd-2p::BFP] I; him-5(e1490)V. Animals were anesthetized with 20 mM levamisole and mounted on their back on 5% agar pads on glass slides. Images were obtained with Nikon CSU-W1spinning disk confocal microscopy with 100× magnification with 5 nm thickness. All images were obtained with same exposure time for the same wave length. (For EM1554, 488 nm laser power 15%, exposure time 50 ms, 561 nm laser power 25%, exposure time 500 ms. For EM1855, 405 nm laser power 30%, exposure time 600 ms, 488 nm laser power 20%, exposure time 200 ms.)

To quantify the protein levels of pre-synaptic markers, all planes for each animal were z-stacked. The circle ROI, or region of interest, contained 205 pixels and was set on the synaptic ring, followed by measuring mean signal intensity. We also quantified the signal intensity of the cytoplasmic fluorescent markers in the same ROI and calculated the pre-synapse/cytoplasmic signal intensity ratio.

Results

Axon trajectory phenotypes of strains carrying single mutations in CAM genes

The trajectories of the RnB neuron processes in wild type, visualized by the cytoplasmic marker, are shown in Fig. 1a and schematically in Fig. 2b. Based on the characteristics of RnB axon morphology, we classified the trajectory defects in mutants into one of four categories (Fig. 2c): (1) anteroposterior guidance defect of axons from R1B-R7B. (2) Circumferential guidance defect of axons from R1B. (3) Number of circumferential commissures from R2B-R7B. (4) Posterior commissures of axons from R8 and 9B. We quantified the percentage of defective worms in each of those four categories (Fig. 2d–g).

The CAM genes and mutations studied in this work are shown in Table 1. We determined the effect of mutations in all of the B-neuron-expressed genes except *pan-1*, which is embryonic lethal. We observed trajectory defects in three of the genes tested, *unc-40, sax-3*, and *fmi-1*. *Unc-40* mutants had significant abnormalities in the dorsoventral guidance system for the formation of all the ray commissures (Fig. 2e, f and h), as reported previously (Hedgecock *et al.* 1990; Jia and Emmons 2006). Significant defects were also observed in anteroposterior guidance and posterior commissures (also referred to as diagonal commissures in Fig. 1b, the commissures containing the processes of ray 8 and ray 9 neurons) (Fig. 2d and g). Although posterior commissures were reported to be unaffected in a previous paper (Jia and Emmons 2006), some were missing when we observed with a confocal microscope. *Sax-3* mutants had abnormal anteroposterior and circumferential axonal projections (Fig. 2d–f). The abnormal anterior axonal projection was often seen in combination with a deletion of the circumferential axon or R1B (Fig. 2h). The lack of circumferential R1B axon seems to be due to a failure of turning of the anterior–posterior axon from the cell body. In *sax-3* mutants, the posterior commissures from rays 8 and 9 were also frequently missing (Fig. 2g and

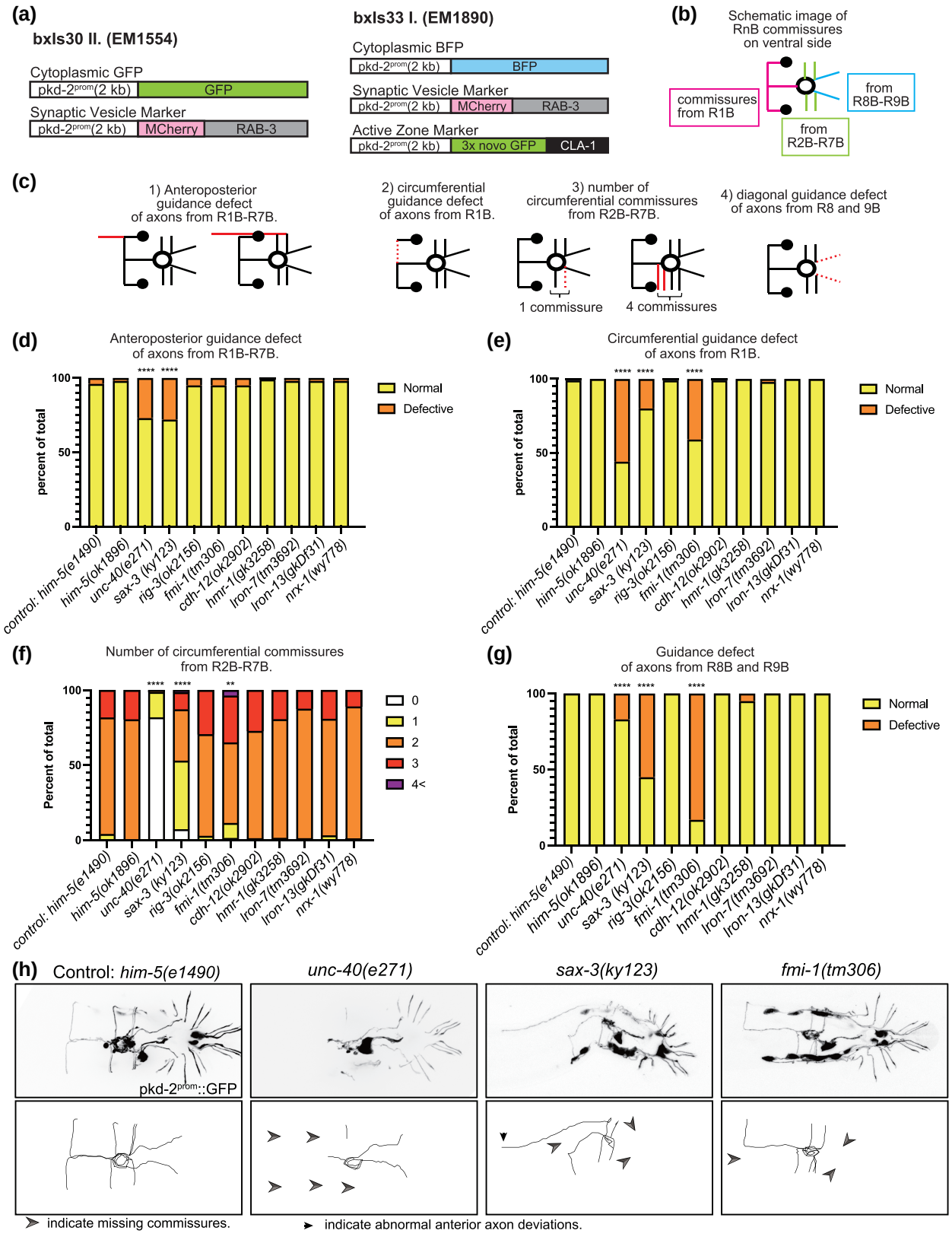

Fig. 2. Trajectories of RnB neurons in CAM mutants. a) Transgenes labeling axon trajectories and pre-synapses in EM1554 *bxIs30*[*pkd-2*^{prom}::GFP, *pkd-2*^{prom}::MCherry-RAB3, *ttx-3*^{prom}::GFP] II; *him-5(e1490)*V and in EM1890 *bxIs33*[*pkd-2*^{prom}::BFP, *pkd-2*^{prom}::MCherry-RAB3, *pkd-2*^{prom}::3xnovoGFP-CLA-1, *ttx-3*^{prom}::MCherry] I; *him-5(e1490)*V. b) A diagram showing typical RnB commissures in wild type. c) Diagrams showing a typical example of each anatomical defect. Red lines indicate the commissure with defect. d–g) Quantified data for defect of anterior-posterior axons (d), of circumferential axon guidance (e), in number of circumferential commissures from R2-7B (f), and of posterior commissures (g). $^{****}P < 0.0001$ vs him-5, $^{**}P < 0.01$ vs him-5, Fisher's exact test. h) Fluorescent images of RnB neurons and HOB neurons (top panels) and traces of commissures from ray neurons (bottom panels) of *him-5(e1490)* control animals and mutant animals. RnB neurons as well as HOB neuron were marked with *pkd-2*^{prom}::GFP. Arrow heads indicate the missing commissures and arrows indicate the abnormal anterior axon deviation.

Table 1. The CAM genes and mutations studied in this work.

Gene name	Allele name	Types of CAMs	Homolog	Type of mutation	References	Axon morphology defects found in this study	Defect of pre-synaptic marker distribution found in this study
CAMs expressed in RnBs							
unc-40	*e271*	Ig protein	DCC	Early stop codon. Reported as a strong loss of function allele.	Hedgecock *et al.* (1990)	anteroposterior guidance defect (R1-R7B) circumferential guidance defect (R1-R7B) diagonal guidance defect(R8-R9B)	increased pre-synaptic marker in circumferrential commissures decreased pre-synaptic marker in synapse ring
sax-3	*ky123*	Ig protein	ROBO	Deletion. Reported as a strong loss of function allele.	Zallen, Yi, and Bargmann (1998); Zallen, Kirch, and Bargmann (1999)	anteroposterior guidance defect (R1-R7B) circumferential guidance defect (R1-R7B) diagonal guidance defect(R8-R9B)	increased pre-synaptic marker in circumferrential commissures
rig-3	*ok2156*	Ig protein	contactin	Deletion. Reported as a strong loss of function allele.	Babu *et al.* (2011)	—	—
fmi-1	*tm306*	Cadherin	Flamingo	Deletion. Reported as a strong loss of function allele.	Najarro *et al.* (2012)	circumferential guidance defect (R1-R7B) diagonal guidance defect(R8-R9B)	—
cdh-12	*ok2902*	Cadherin	nematode specific	No phenotype is reported. Frameshift deletion results in an early stop codon.	—	—	—
hmr-1b	*gk3258*	Cadherin	E-cadherin	No phenotype is reported. Frameshift deletion results in an early stop codon. The deletion only affect the long form of hmr-1(hmr-1b). The short form of hmr-1(hmr-1a) is thought to be intact.	—	—	decreased pre-synaptic marker in synapse ring
nrx-1	*wy778*	Neurexin	Neurexin	Deletion. Reported as a strong loss of function allele.	Maro *et al.* (2015); Kurshan *et al.* (2018)	—	—
lron-7	*tm3692*	LRR protein	OPTC	No phenotype is reported. Non-frameshifting deletion covers almost the entire LRR domain.	—	—	—
lron-13	*gkDf31*	LRR protein	nematode specific	No phenotype is reported. Frameshift deletion results in an early stop codon.	—	—	—
CAMSs expressed in RnAs							
sax-7	*nj48*	Ig protein	*L1CAM*	Deletion. Reported as a strong loss of function allele. This deletion affect both long and short isoforms.	Sasakura *et al.* (2005)	—	—
bam-2	*cy6*	Neurexin	Neurexin related	Nonsense mutation. Predicted as a genetic null allele.	Colavita and Tessier-Lavigne (2003)	—	—
tol-1	*nr2013*	LRR protein	Toll-like receptors	Deletion. Predicted as a null allele.	Pujol *et al.* (2001)	circumferrential guidance defect(R2-R7B)	—

h). Mutation in *fmi-1*/flamingo resulted in a deficit of the circumferential commissures (Fig. 2e, f, and h), and most notably, an absence of the posterior commissures in almost all animals (Fig. 2g and h).

For all of the remaining genes, *rig-3*, *cdh-12*, *hmr-1*, *lron-7*, *lron-13*, and *nrx-1*, animals containing single mutations had no significant defects in axon trajectories when compared to wild type (Fig. 2d–g).

Axon trajectory phenotypes of strains carrying multiple mutations in CAM genes

In view of the lack of effects of single mutations in most of the genes, we asked whether this was due to redundancy of their activities by examining double and multiple mutants. We found that this does not appear to be the case. Since *rig-3* and *lron-7* loci are close and we could not create this double, we created two quintuple mutants (*hmr-1*; *cdh-12 lron-13*; *nrx-1*; *lron-7* and *hmr-1*; *cdh-12 lron-13*; *nrx-1*; *rig-3*). In all of the strains carrying multiple mutations in genes with no single effect, there were no significant abnormalities (Fig. 3a–d).

Next, we crossed the strains with observable phenotypes, *sax-3* and *fmi-1*, into the strains with no obvious phenotype to look for genetic interactions (enhancement or suppression) (Fig. 3e–j). We found that the *hmr-1* mutant significantly enhanced the axon guidance defects in the circumferential commissures in a *sax-3* mutant (Fig. 3f and g), indicating that *hmr-1* and *sax-3* have redundant functions. In addition, *lron-13* and *lron-7* suppressed axon guidance defects in *sax-3* and *fmi-1*, respectively (Fig. 3e and i). These mutants have not been reported to have any significant phenotypes, but they may be involved in the regulation of axon guidance in cooperation with other CAMs.

Effects of mutations in genes expressed in RnA neurons on axon trajectories of RnB neurons

RnA and RnB neuron processes run side by side from the dendrites in the rays through circumferential commissure fascicles until they enter the pre-anal ganglion (Fig. 1b) (Jia and Emmons 2006; Jarrell *et al.* 2012; Cook *et al.* 2019). We, therefore, examined whether CAMs expressed in RnA neurons affect axon guidance in RnB neurons. Although many CAMs are expressed in the RnA neurons (Fig. 1c), we focused on the effects of four genes (*casy-1*, *bam-2*, *sax-7*, and *tol-1*) that are widely expressed in most of the RnA neurons. Single mutations in *casy-1*, *bam-2*, and *sax-7* showed no abnormalities in the morphology of the RnB neurons (Fig. 4a–d). In the *tol-1* mutant, there was a significant increase in the number of commissures from Ray2–7 (Fig. 4c). This result suggests that *tol-1* may be involved in the fasciculation of the circumferential commissures.

SAX-7 has been reported to interact with SAX-3 in axonal fasciculation (Chen *et al.* 2019). We therefore asked whether these proteins acted together in a single pathway for ray fasciculation or separately by determining whether mutation in *sax-7*, expressed in RnA, would enhance the defect of RnB axon trajectory in a double mutant with *sax-3*, expressed in RnB (Fig. 4e–g). We found the *sax-7* mutation significantly enhanced the RnB abnormalities in the circumferential commissure of the *sax-3* mutant (Fig. 4f). This suggests that these two proteins have independent and apparently somewhat redundant functions in promoting fasciculation of their respective neuron processes in the commissures.

In view of this possibility, we tested for a possible reciprocal effect on RnA trajectories of mutations in those RnB-expressed genes that affected RnB trajectories. We visualized a subset of RnA neurons using DAT-1p::GFP expressed in R5A, R7A, and R9A (Fig. 4h). We observed abnormalities in RnA neurite trajectories in both *sax-3* and *fmi-1* mutants similar to those observed in the RnB neurons (Fig. 4i and j). Thus, each of the two neuron types appears to promote the trajectories of the other type, consistent with their co-fasciculation in the outgrowing commissures.

Effects of mutations in CAM genes on synapse formation

CAMs are involved not only in axon guidance but also in synapse formation (Shen and Bargmann 2003; Dalva *et al.* 2007; Kim and Emmons 2017; Kurshan *et al.* 2018; Lázaro-Peña *et al.* 2018; Philbrook *et al.* 2018; Südhof 2018). We visualized RnB synapses with fluorescent markers localized respectively to synaptic vesicles (RAB-3) and pre-synaptic densities (CLA-1) (Fig. 2a). RAB-3 signals and CLA-1 signals are mostly co-localized but sometimes are seen in different distributions. This suggests that synaptic vesicles and active zone proteins may be localized separately. Both reporter genes showed a pattern of fluorescence consistent with RnB pre-synapses as described by electron microscopy (Jarrell *et al.* 2012) (Fig. 5a and b). Most RnB synapses are in the pre-anal ganglion, where the densest fluorescence appears as a ring, dubbed here the "synaptic ring." In addition, consistent with the mixed axonal/dendritic character of most *C. elegans* neurons, they receive a similar amount of input from other neurons. These post-synapses are not visualized here. Multiple pre-synapses were also observed within the pre-anal ganglion along the midline axon and in the lumbar ganglia, but few in circumferential commissures and, in the case of the RAB-3 reporter, almost none inside ray structures. By contrast, the GFP::CLA-1 reporter indicated the presence of pre-synaptic densities inside ray structures (Fig. 5b). We examined EM images of the rays and found synapse-like structures with high electron density within the ray dendrites in the rays (Fig. 5c). Altogether, in the EM reconstruction of a single adult male, the RnB neurons form 1,143 chemical synapses onto 123 other sensory neurons, including other ray neurons, interneurons, and motor neurons, most of which are in the pre-anal ganglion (Jarrell *et al.* 2012) (Fig. 1b).

To assay the amount of synapse formation, in order to control for different levels of gene expression we determined the ratio of signal intensity between the synaptic signals (RAB-3::mCherry for *bxIs30II*, RAB-3::mCherry and GFP::CLA-1 for *bxIs33I*) and the cytoplasmic signals (GFP for *bxIs30II.*, BFP for *bxIs33I*) (Fig. 5d–f). In *unc-40* and *sax-3* mutants, both pre-synaptic marker ratios were increased in circumferential commissures (Fig. 5, d and g). This suggests accumulation of synaptic proteins in processes that have failed to reach their targets. In the *unc-40* mutant, the RAB-3-MCherry ratio decreased in the synaptic ring region but the GFP-CLA1 ratio increased (Fig. 5e and h). Thus CLA-1 protein may accumulate within those few processes that reach the target area. In the *hmr-1(gk3258)* mutant, the RAB-3::mCherry signal ratio was decreased in the synaptic ring, whereas there was no significant increase or decrease within circumferential commissures (Fig. 5d–f). (The CLA-1 reporter could not be tested because of proximity of the mutation to the transgene insertion site.) Thus, *hmr-1* may be involved in accumulation of synaptic vesicles. Besides these, there were no other deviations from wild type ratios in the single and multiple mutants. In none of the mutants was there any significant presynapse signal ratio change in midline axons (Fig. 5f).

These results indicate a limited effect of mutations in RnB-expressed CAM genes on accumulation of pre-synaptic components within the neuronal processes. Whether this indicates these CAM genes play no role in recognition of synaptic targets and formation of synapses or that synaptic components accumulate in the absence of target recognition and synapse formation cannot be determined.

SAX-3 regulates circumferential axon guidance in a *slt-1* independent manner

For two of the genes we studied, *sax-3* and *fmi-1*, interacting partners or pathway components are known in other systems. For SAX-3/ROBO, it has been demonstrated in many species that Slit, a secreted LRR protein, functions as a ligand (Brose *et al.* 1999; Zallen *et al.* 1999; Hao *et al.* 2001; Dickinson and Duncan 2010; Tong *et al.* 2019; Jiang *et al.* 2022). In our expression dataset, *slt-1* is mainly expressed in ALN neurons and dorsal body wall

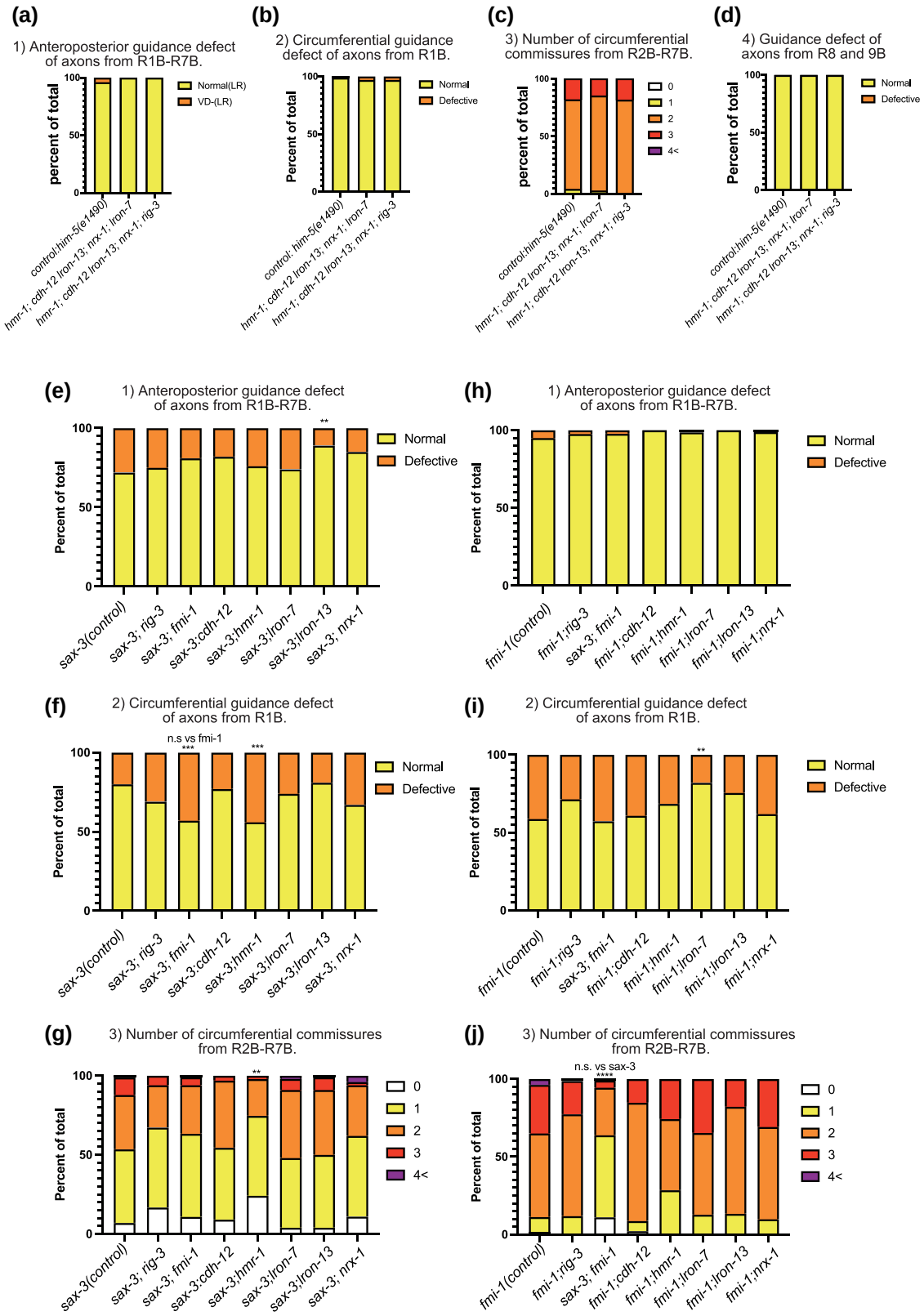

Fig. 3. Genetic interactions between CAMs expressed in RnB neurons. a–d) Percentage of defect of anterior-posterior axon guidance (a), percentage of defect of circumferential R1B axon guidance (b), number of circumferential commissures from R2-7B (c), and percentage of defect of posterior commissures (d) for quintuple mutants of CAMs expressed in RnB neurons. e, f) Percentage of defects of anterior-posterior axon guidance (e), percentage of defects of circumferential R1B axon guidance (f), and number of circumferential commissures from R2-7B (g) for double mutants of *sax-3* and CAMs expressed in RnB neurons. h–j) Percentage of defective anterior-posterior axon guidance (h), percentage of defective circumferential R1B axon guidance (i), and number of circumferential commissures from R2-7B (j) for double mutants of *fmi-1* and CAMs expressed in RnB neurons. ****$P < 0.0001$ vs control, *** $P < 0.001$ vs control, **$P < 0.01$ vs control, *$P < 0.05$ vs control, n.s $P > 0.05$, Fisher's exact test.

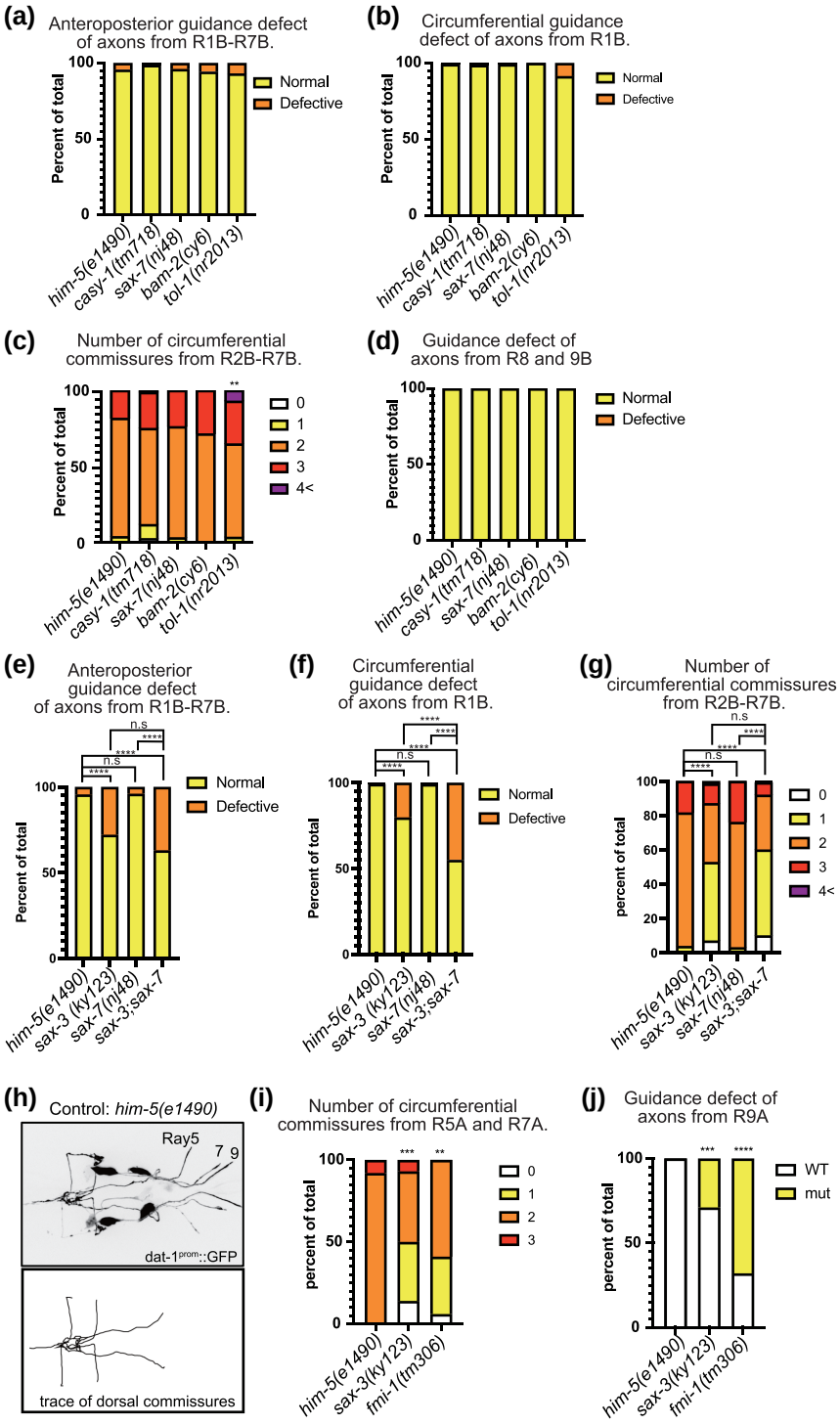

Fig. 4. *sax-3* and *fmi-1* mutants showed abnormal RnA neuron morphology. a–d) Percentage of defective anterior-posterior axon guidance (a), percentage of defective circumferential R1B axon guidance (b), number of circumferential commissures from R2-7B (c), and percentage of defective diagonal commissures for mutants of CAMs expressed in RnA neurons (d). e–g) Percentage of defective anterior-posterior axon guidance (e), percentage of defective circumferential R1B axon guidance (f), and number of circumferential commissures from R2-7B (g) for *sax-3*, *sax-7*, and *sax-3; sax-7* mutants are shown. h) Fluorescent images of R5A, R7A, R9A neurons (top panels) and traces of commissures from Ray neurons (bottom panels) of *him-5(e1490)* control animal. RnA neurons were marked with *dat-1*^{prom}::GFP. i–j) Percentage of number of commissures from R5, 7A (i) and percentage of defective diagonal commissures (j) for sax-3 and fmi-1 mutants are shown. ****$P < 0.0001$ vs him-5, *** $P < 0.001$ vs him-5, **$P < 0.01$ vs him-5, Fisher's exact test.

muscles. We tested whether *slt-1* is involved in RnB axon guidance and found that *slt-1* null mutants showed abnormal anterior axon projections and loss of circumferential axons, which were also observed in *sax-3* mutants (Fig. 6a and b). The absence of *slt-1* did not enhance the *sax-3* mutant phenotype in a double mutant, consistent with SLT-1 functioning as a ligand for SAX-3. By contrast, *slt-1* single mutation did not show any significant abnormality in the number of commissures from R2-7B (Fig. 6c). This result and the

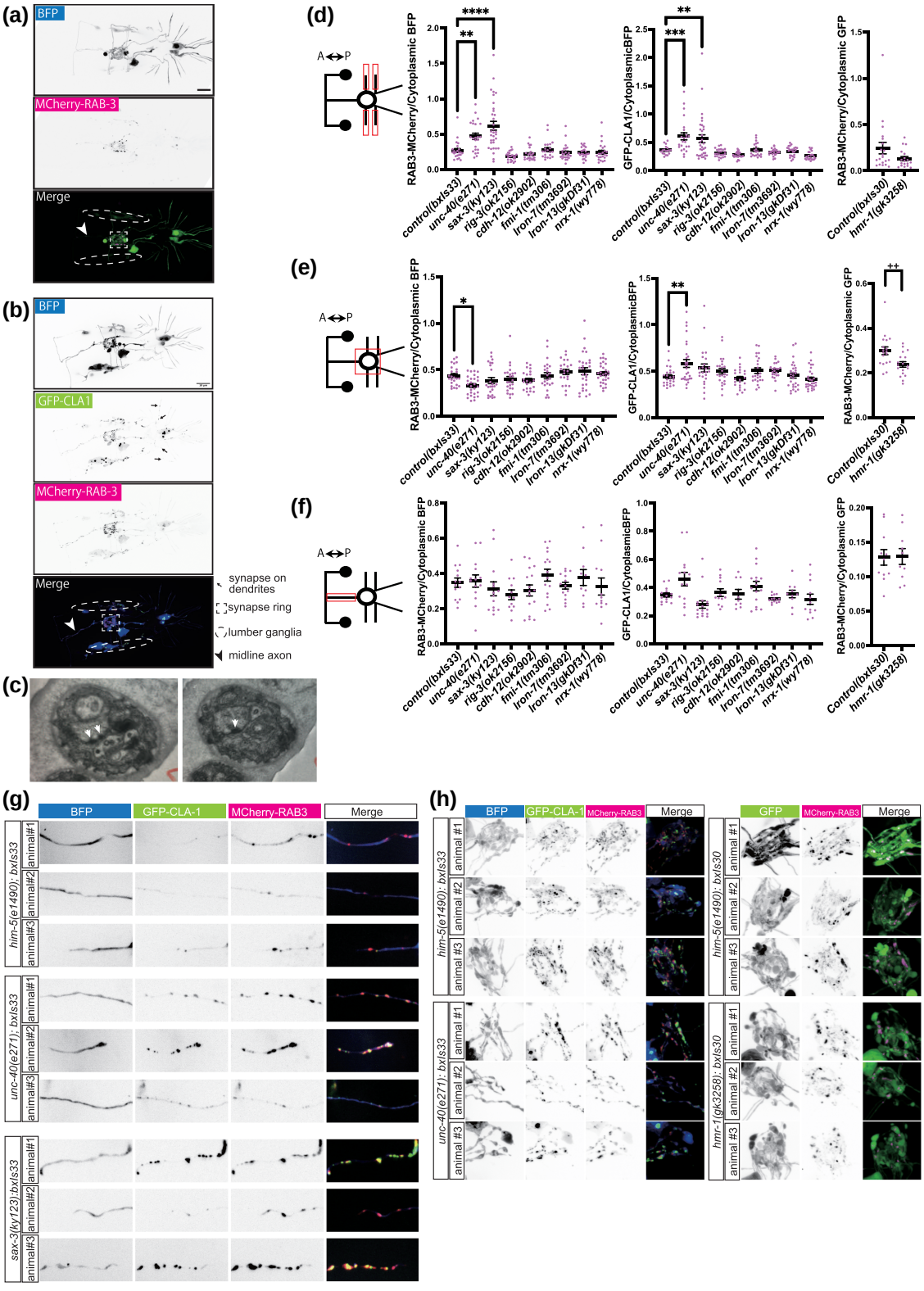

Fig. 5. Expression of synaptic markers in CAM gene mutants. a) Fluorescent images of EM1554. Broken-line square, broken-line oval, and arrowhead represent synaptic ring, lumbar ganglia, and midline axon, respectively. b) Fluorescent images of EM1890. Black arrow, broken-line square, broken-line oval, and arrow represent synapses on ray dendrites, synaptic ring, lumber ganglia, and midline axon, respectively. c) Electron microscopy images of two consecutive sections. The white arrows indicate synapse-like structures with high electron density. d–f) Schematic images and quantified data of pre-synaptic markers in (d) Circumferential commissures, e) Synaptic ring, and (f) midline axon. Data of left panels show signal intensity ratio of 3xnovoGFP-CLA1/cytoplasmic BFP for each mutant with *bxIs*33. Center panels show signal intensity ratio of RAB3-MCherry/cytoplasmic BFP for each mutant with *bxIs*33. Right panels show signal intensity ratio of RAB3-MCherry/cytoplasmic GFP for each mutant with *bxIs*30. Red boxes in the schematic images indicate the region of interest. ****$P < 0.0001$ vs control, ***$P < 0.001$ vs control, **$P < 0.01$ vs control, multiple comparison test. ++$P < 0.01$ vs control, t-test. g) Fluorescent images of circumferential commissures in mutants with *bxIs*33 or *bxIs*30. h) Fluorescent images of synaptic ring in mutants with *bxIs*33.

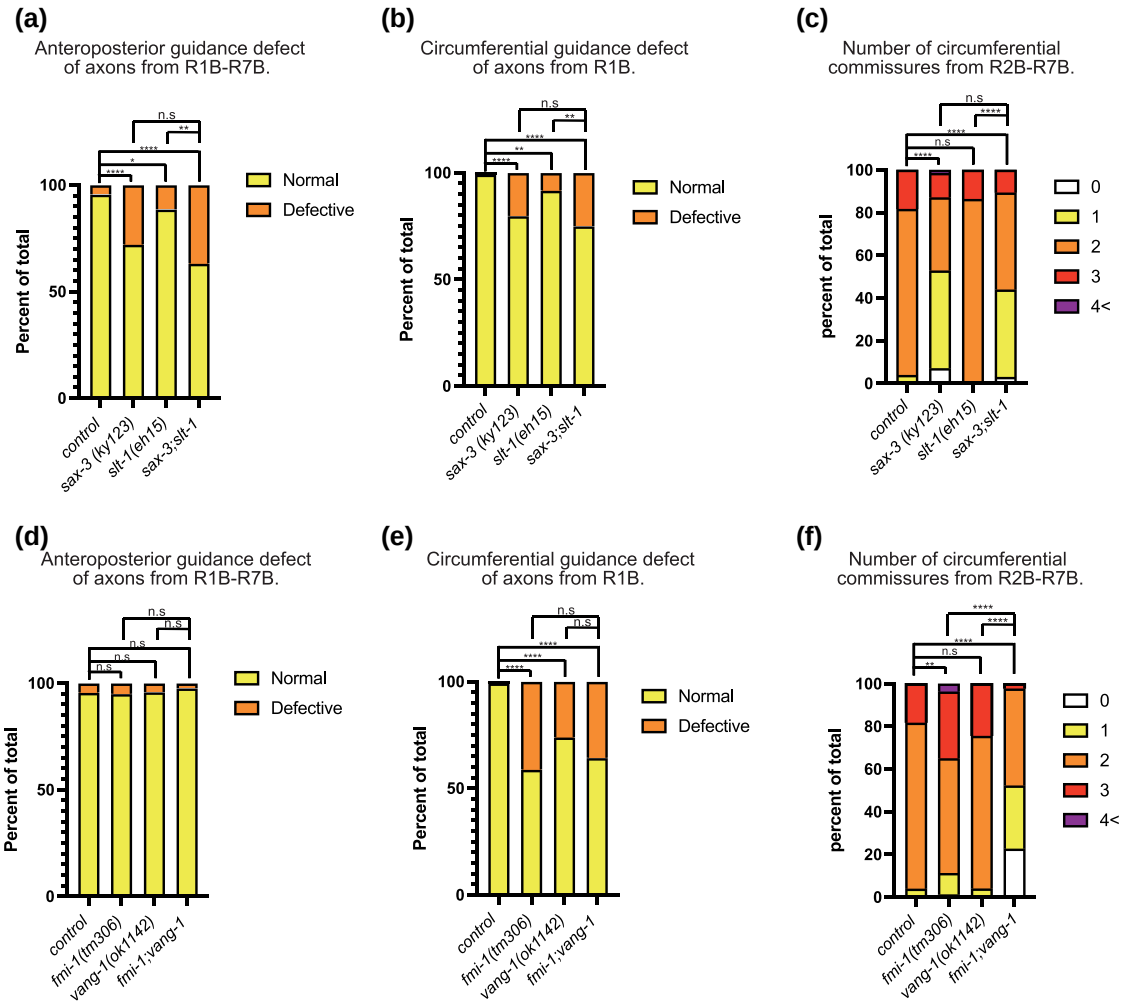

Fig. 6. Genetic interactions between *sax-3*, *fmi-1*, and their known interacting partners. a–c) Percentage of defective anterior-posterior axon guidance (a), percentage of defective circumferential R1B axon guidance (b), and number of circumferential commissures from R2-7B (c) for *sax-3*, *slt-1*, and *sax-3; slt-1* mutants. d–f) Percentage of defective anterior-posterior axon guidance (d), percentage of defective circumferential R1B axon guidance (e), and number of circumferential commissures from R2-7B (f) for *fmi-1*, *vang-1*, *and fmi-1; vang-1* mutants. ****$P < 0.0001$, **$P < 0.01$, *$P < 0.05$, n.s $P > 0.05$, Fisher's exact test.

lesser overall severity of the *slt-1* null mutant phenotype compared to the *sax-3* null mutant phenotype indicate that molecules other than SLT-1 may function as ligands for SAX-3 in RnB axon guidance.

FMI-1 regulates RnB axon guidance both in the PCP pathway and PCP-independent pathway

In Drosophila, Flamingo, a homolog of *fmi-1*, was previously reported to work together with Van Goh and Frizzled to regulate the PCP (planar cell polarity) pathway (Usui *et al.* 1999). We tested whether the PCP pathway genes are involved in RnB axon guidance (Fig. 6d–f). The lack of the circumferential axon from R1B was occasionally seen in a *vang-1* mutant (homolog of Van Goh) (Fig. 6e). This phenotype was not enhanced by *fmi-1* null mutant (Fig. 6e), indicating *fmi-1* and *vang-1* work in the same pathway. On the other hand, the *fmi-1; vang-1* double mutant showed a significantly more severe phenotype than the *fmi-1* mutant alone in circumferential commissures from R2-7 (Fig. 6f). These results suggest that *fmi-1* and *vang-1* regulate the morphology of RnB neurons within the same pathway as well as in parallel pathways.

Discussion

C. elegans ray sensory neurons provide an excellent opportunity to identify the factors that determine neuronal wiring selectivity. Genes involved in formation of the two neuron types and that specify ray neuron identities have been described, including transcription factors and signaling pathways (Baird *et al.* 1991; Chow and Emmons 1994). Regulatory genes must act by controlling the expression of effector genes that function during morphogenesis. Here, we examined the class of genes thought to specify the cell surface labels that govern cell–cell recognition for synapse formation. Like other neurons in the *C. elegans* nervous system, ray sensory neurons express multiple CAMs, including many conserved across species (Hahn and Emmons 2003; Taylor *et al.* 2021; this laboratory unpublished). Reflecting an aspect of ray identity, the combination expressed by the neurons in each ray pair differs (Fig. 1c). The same genes are expressed in other combinations across the entire set of neurons and muscles in the posterior nervous system, indeed, across the entire animal in all tissues, reflecting their presumptive function as neutral cell labels, that is, labels not associated with any particular cell type or cell fate (Taylor *et al.* 2021; this laboratory unpublished).

Our primary result reported here is that mutations in the CAM genes expressed by the ray neurons have surprisingly limited effects on two aspects of ray neuron phenotype: axon trajectories and accumulation of pre-synaptic proteins in axonal processes. General absence of effects on axon trajectories reflects the robustness of the mechanisms that guide formation of the structure. For example, we found that SAX-3/ROBO and SAX-7/L1CAM each appear to independently contribute to fasciculation of the RnB and RnA circumferential processes.

In this study, we analyzed the known interacting partners for *sax-3* and *fmi-1*, and found that the mutant of *slt-1*, a well-known SAX-3 interacting partner, showed a weaker phenotype compared to *sax-3* mutants, strongly suggesting the existence of ligands of SAX-3 other than SLT-1. The NELL protein has recently been reported as a ligand for ROBO (Yamamoto *et al.* 2019; Pak *et al.* 2020), but no nematode homolog has been reported so far. We also found that lack of *vang-1*/VanGoh enhanced the *fmi-1* phenotype in circumferential commissures from R2-7, suggesting that *vang-1* and *fmi-1* function in a parallel manner and the existence of a ligand for FMI-1 other than VANG-1. Further research on ray neuron development thus may lead to the discovery of novel ligands for *sax-3* and *fmi-1*.

We observed increased synaptic proteins in circumferential commissures in some mutants. The accumulation of synapse proteins was examined in three different compartments. The amounts of synaptic proteins at the three locations did not coincide. For example, in the *sax-3* mutant, synapse protein accumulation was increased in the circumferential commissure, but not in the synaptic ring and longitudinal commissure (Fig. 6d–f). This may suggest that the degree of contribution of CAMs to synaptogenesis varies from compartment to compartment within the same nerve.

There is precedent for synapses between sensory dendrites as we report here between ray sensory neuron dendrites. Pre-synaptic densities are observed within the sensory amphid bundles in the head (Cook *et al.* 2019). The functions of such dendrite–dendrite synapses are unknown but may simply be a part of the complex set of connections among sensory neurons seen broadly across the connectome. Alternatively, they could represent sites of release of extracellular vesicles, which occurs from the ray neurons as well as other *C. elegans* sensory dendrites (Wang *et al.* 2014).

Ray sensory neurons send axonal growth cones into a preexisting, complex neuropil where they seek out and find their post-synaptic partners. The question we have addressed here is how molecular cell-cell recognition occurs to guide this synaptogenesis. Previously we have shown that elimination of a specific sugar modification on the heparan sulfate proteoglycan glypican affected the formation of synapses between the ray B-type neurons and three of their major post-synaptic targets, the three male-specific EF interneurons (Lázaro-Peña *et al.* 2018). In a background containing a mutation in a gene encoding a sugar modification enzyme, the amount of synapse formation to the EF neurons was reduced although not eliminated. Intriguingly, the level of fluorescently labeled RAB-3 within the RnB target area increased in this background. Effects on accumulation of synaptic proteins probably reflects the fact that assembly and transport of such components to sites of expected synapse formation may be to some degree independent of target recognition and synapse formation (Kurshan and Shen 2019). The correlation of apparent accumulation of pre-synaptic components with loss of synapse formation in this previous example suggests that the apparent accumulation observed here could likewise indicate a loss of synapses. The question can be addressed with the methods that demonstrate interaction of pre- and post-synaptic cells, GRASP or iBLINC (Feinberg *et al.* 2008; Desbois *et al.* 2015).

Acknowledgements

We thank H. Bülow and D. Hall for technical advice and D. Hall for assistance in examining electron micrographs for evidence of synaptic densities within rays. The plasmid containing CLA-1-GFP was a kind gift of P Kurshan. *C. elegans* strains were provided by the CGC, which is funded by NIH Office of Research Infrastructure Programs (P40 0D010440), and NBRP (Japan).

Funding

This work was supported by National Institutes of Health grants from National Institute for Human Development (P30HD071593 to S.W.E.), National Institute for Mental Health (R01MH112689 to S.W.E.), National Institute of General Medical Sciences (R01GM066897 to S.W.E.), and Japan Society for the Promotion of Science Overseas Research Fellowships to N.S. N.S. was supported by the Analytical Imaging Facility of the Albert Einstein Cancer Center (P30 CA013330).

Conflicts of interest

None declared.

Data availability

Strains and plasmids are available upon request. The datasets and imaging data generated and/or analyzed during the current study are available from the corresponding author on reasonable request.

Supplemental material available at G3 online.

Literature cited

Babu K, Hu Z, Chien SC, Garriga G, Kaplan JM. The immunoglobulin super family protein RIG-3 prevents synaptic potentiation and regulates Wnt signaling. Neuron. 2011;71(1):103–116. doi:10.1016/j.neuron.2011.05.034.

Baird SE, Fitch DH, Kassem IA, Emmons SW. Pattern formation in the nematode epidermis: determination of the arrangement of peripheral sense organs in the C. elegans male tail. Development. 1991;113(2):515–526. doi:10.1242/dev.113.2.515.

Barr MM, Sternberg PW. A polycystic kidney-disease gene homologue required for male mating behaviour in C. elegans. Nature. 1999;401(6751):386–389. doi:10.1038/43913.

Brenner S. The genetics of Caenorhabditis elegans. Genetics. 1974;77(1):71–94. doi:10.1093/genetics/77.1.71.

Brose K, Bland KS, Wang KH, Arnott D, Henzel W, Goodman CS, Tessier-Lavigne M, Kidd T. Slit proteins bind Robo receptors and have an evolutionarily conserved role in repulsive axon guidance. Cell. 1999;96(6):795–806. doi:10.1016/S0092-8674(00)80590-5.

Broverman SA, Meneely PM. Meiotic mutants that cause a polar decrease in recombination on the X chromosome in Caenorhabditis elegans. Genetics. 1994;136(1):119–127. doi:10.1093/genetics/136.1.119.

Carrillo RA, Özkan E, Menon KP, Nagarkar-Jaiswal S, Lee P-T, Jeon M, Birnbaum ME, Bellen HJ, Garcia KC, Zinn K. Control of synaptic

connectivity by a network of drosophila IgSF cell surface proteins. Cell. 2015;163(7):1770–1782. doi:10.1016/j.cell.2015.11.022.

Chen C-H, Hsu H-W, Chang Y-H, Pan C-L. Adhesive L1CAM-robo signaling aligns growth cone F-actin dynamics to promote axon-dendrite fasciculation in C. elegans. Dev Cell. 2019;49(3):490–491. doi:10.1016/j.devcel.2019.04.028.

Chow KL, Emmons SW. HOM-C/Hox genes and four interacting loci determine the morphogenetic properties of single cells in the nematode male tail. Development. 1994;120(9):2579–2592. doi:10.1242/dev.120.9.2579.

Cook SJ, Jarrell TA, Brittin CA, Wang Y, Bloniarz AE, Yakovlev MA, Nguyen KCQ, Tang LT-H, Bayer EA, Duerr JS, *et al.* Whole-animal connectomes of both Caenorhabditis elegans sexes. Nature. 2019;571(7763):63–71. doi:10.1038/s41586-019-1352-7.

Dalva MB, McClelland AC, Kayser MS. Cell adhesion molecules: signalling functions at the synapse. Nat Rev Neurosci. 2007;8(3):206–220. doi:10.1038/nrn2075.

Desbois M, Cook SJ, Emmons SW, Bülow HE. Directional trans-synaptic labeling of specific neuronal connections in live animals. Genetics. 2015;200(3):697–705. doi:10.1534/genetics.115.177006.

Dickinson RE, Duncan WC. The SLIT–ROBO pathway: a regulator of cell function with implications for the reproductive system. Reproduction. 2010;139(4):697–704. doi:10.1530/REP-10-0017.

Feinberg EH, Vanhoven MK, Bendesky A, Wang G, Fetter RD, Shen K, Bargmann CI. GFP reconstitution Across Synaptic Partners (GRASP) defines cell contacts and synapses in living nervous systems. Neuron. 2008;57(3):353–363. doi:10.1016/j.neuron.2007.11.030.

Hahn AC, Emmons SW. The roles of an ephrin and a semaphorin in patterning cell-cell contacts in C. elegans sensory organ development. Dev Biol. 2003;256(2):379–388. doi:10.1016/S0012-1606(02)00129-X.

Hao JC, Yu TW, Fujisawa K, Culotti JG, Gengyo-Ando K, Mitani S, Moulder G, Barstead R, Tessier-Lavigne M, Bargmann CI. C. elegans slit acts in midline, dorsal-ventral, and anterior-posterior guidance via the SAX-3/Robo receptor. Neuron. 2001;32(1):25–38. doi:10.1016/S0896-6273(01)00448-2.

Hedgecock EM, Culotti JG, Hall DH. The unc-5, unc-6, and unc-40 genes guide circumferential migrations of pioneer axons and mesodermal cells on the epidermis in C. elegans. Neuron. 1990;4(1):61–85. doi:10.1016/0896-6273(90)90444-K.

Jarrell TA, Wang Y, Bloniarz AE, Brittin CA, Xu M, Thomson JN, Albertson DG, Hall DH, Emmons SW. The connectome of a decision-making neural network. Science. 2012;337(6093):437–444. doi:10.1126/science.1221762.

Jia L, Emmons SW. Genes that control ray sensory neuron axon development in the Caenorhabditis elegans male. Genetics. 2006;173(3):1241–1258. doi:10.1534/genetics.106.057000.

Jiang L, Sun J, Huang D. Role of slit/Robo signaling pathway in bone metabolism. Int J Biol Sci. 2022;18(3):1303–1312. doi:10.7150/ijbs.66931.

Kim B, Emmons SW. Multiple conserved cell adhesion protein interactions mediate neural wiring of a sensory circuit in C. elegans. Elife. 2017;6:e29257. doi:10.7554/eLife.29257.

Kurshan PT, Merrill SA, Dong Y, Ding C, Hammarlund M, Bai J, Jorgensen EM, Shen K. γ-Neurexin and frizzled mediate parallel synapse assembly pathways antagonized by receptor endocytosis. Neuron. 2018;100(1):150–166.e4. doi:10.1016/j.neuron.2018.09.007.

Kurshan PT, Shen K. Synaptogenic pathways. Curr Opin Neurobiol. 2019;57:156–162. doi:10.1016/j.conb.2019.03.005.

Lázaro-Peña MI, Díaz-Balzac CA, Bülow HE, Emmons SW. Synaptogenesis is modulated by heparan sulfate in Caenorhabditis elegans. Genetics. 2018;209(1):195–208. doi:10.1534/genetics.118.300837.

Lints R, Jia L, Kim K, Li C, Emmons SW. Axial patterning of C. elegans male sensilla identities by selector genes. Dev Biol. 2004;269(1):137–151. doi:10.1016/j.ydbio.2004.01.021.

Maro GS, Gao S, Olechwier AM, Hung WL, Liu M, Özkan E, Zhen M, Shen K. MADD-4/Punctin and Neurexin Organize C. elegans GABAergic Postsynapses through Neuroligin. Neuron. 2015;86(6):1420–1432. doi:10.1016/j.neuron.2015.05.015.

Mello CC, Kramer JM, Stinchcomb D, Ambros V. Efficient gene transfer in C.elegans: extrachromosomal maintenance and integration of transforming sequences. EMBO J. 1991;10(12):3959–3970. doi:10.1002/j.1460-2075.1991.tb04966.x.

Najarro EH, Wong L, Zhen M, Carpio EM, Goncharov A, Garriga G, Lundquist EA, Ackley BD. Caenorhabditis elegans flamingo cadherin fmi-1 regulates GABAergic neuronal development. J Neurosci. 2012;32(12):4196–4211. doi:10.1523/JNEUROSCI.3094-11.2012.

Nonet ML, Staunton JE, Kilgard MP, Fergestad T, Hartwieg E, Horvitz HR, Jorgensen EM, Meyer BJ. Caenorhabditis elegans rab-3 mutant synapses exhibit impaired function and are partially depleted of vesicles. J Neurosci. 1997;17(21):8061–8073. doi:10.1523/JNEUROSCI.17-21-08061.1997.

Pak JS, DeLoughery ZJ, Wang J, Acharya N, Park Y, Jaworski A, Özkan E. NELL2-Robo3 complex structure reveals mechanisms of receptor activation for axon guidance. Nat Commun. 2020;11(1):1489. doi:10.1038/s41467-020-15211-1.

Philbrook A, Ramachandran S, Lambert CM, Oliver D, Florman J, Alkema MJ, Lemons M, Francis MM. Neurexin directs partner-specific synaptic connectivity in C. elegans. Elife. 2018;7:e35692. doi:10.7554/eLife.35692.

Pujol N, Link EM, Liu LX, Kurz CL, Alloing G, Tan MW, Ray KP, Solari R, Johnson CD, Ewbank JJ. A reverse genetic analysis of components of the Toll signaling pathway in Caenorhabditis elegans. Curr Biol. 2001;11(11):809–821. doi:10.1016/S0960-9822(01)00241-X.

Salzberg Y, Díaz-Balzac CA, Ramirez-Suarez NJ, Attreed M, Tecle E, Desbois M, Kaprielian Z, Bülow HE. Skin-derived cues control arborization of sensory dendrites in Caenorhabditis elegans. Cell. 2013;155(2):308–320. doi:10.1016/j.cell.2013.08.058.

Sasakura H, Inada H, Kuhara A, Fusaoka E, Takemoto D, Takeuchi K, Mori I. Maintenance of neuronal positions in organized ganglia by SAX-7, a Caenorhabditis elegans homologue of L1. EMBO J. 2005;24(7):1477–1488. doi:10.1038/sj.emboj.7600621.

Shah PK, Tanner MR, Kovacevic I, Rankin A, Marshall TE, Noblett N, Tran NN, Roenspies T, Hung J, Chen Z, *et al.* PCP And SAX-3/Robo pathways cooperate to regulate convergent extension-based nerve cord assembly in C. elegans. Dev Cell. 2017;41(2):195–203.e3. doi:10.1016/j.devcel.2017.03.024.

Shen K, Bargmann CI. The immunoglobulin superfamily protein SYG-1 determines the location of specific synapses in C. elegans. Cell. 2003;112(5):619–630. doi:10.1016/S0092-8674(03)00113-2.

Shen K, Fetter RD, Bargmann CI. Synaptic specificity is generated by the synaptic guidepost protein SYG-2 and its receptor, SYG-1. Cell. 2004;117(4):553. doi:10.1016/S0092-8674(04)00407-6.

Sperry RW. Chemoaffinity in the orderly growth of nerve fiber patterns and connections. Proc Natl Acad Sci U S A. 1963;50(4):703–710. doi:10.1073/pnas.50.4.703.

Südhof TC. Towards an understanding of synapse formation. Neuron. 2018;100(2):276–293. doi:10.1016/j.neuron.2018.09.040.

Sulston JE, Albertson DG, Thomson JN. The Caenorhabditis elegans male: postembryonic development of nongonadal structures. Dev Biol. 1980;78(2):542–576. doi:10.1016/0012-1606(80)90352-8.

Taylor SR, Santpere G, Weinreb A, Barrett A, Reilly MB, Xu C, Varol E, Oikonomou P, Glenwinkel L, McWhirter R, *et al.* Molecular topography of an entire nervous system. Cell. 2021;184(16): 4329–4347.e23. doi:10.1016/j.cell.2021.06.023.

Tong M, Jun T, Nie Y, Hao J, Fan D. The role of the Slit/Robo signaling pathway. J Cancer. 2019;10(12):2694–2705. doi:10.7150/jca.31877.

Usui T, Shima Y, Shimada Y, Hirano S, Burgess RW, Schwarz TL, Takeichi M, Uemura T. Flamingo, a seven-pass transmembrane cadherin, regulates planar cell polarity under the control of Frizzled. Cell. 1999;98(5):585–595. doi:10.1016/S0092-8674(00)80046-X.

Wang J, Silva M, Haas LA, Morsci NS, Nguyen KCQ, Hall DH, Barr MM. C. elegans ciliated sensory neurons release extracellular vesicles that function in animal communication. Curr Biol. 2014;24(5): 519–525. doi:10.1016/j.cub.2014.01.002.

White JG, Southgate E, Thomson JN, Brenner S. The structure of the nervous system of the nematode Caenorhabditis elegans. Philos Trans R Soc Lond B Biol Sci. 1986;314(1165):1–340. doi:10.1098/rstb.1986.0056.

Xuan Z, Manning L, Nelson J, Richmond JE, Colón-Ramos DA, Shen K, Kurshan PT. Clarinet (CLA-1), a novel active zone protein required for synaptic vesicle clustering and release. Elife. 2017;6: e29276. doi:10.7554/eLife.29276.

Yamagata M, Weiner JA, Sanes JR. Sidekicks: synaptic adhesion molecules that promote lamina-specific connectivity in the retina. Cell. 2002;110(5):649–660. doi:10.1016/S0092-8674(02)00910-8.

Yamamoto N, Kashiwagi M, Ishihara M, Kojima T, Maturana AD, Kuroda S, Niimi T. Robo2 contains a cryptic binding site for neural EGFL-like (NELL) protein 1/2. J Biol Chem. 2019;294(12):4693–4703. doi:10.1074/jbc.RA118.005819.

Zallen JA, Kirch SA, Bargmann CI. Genes required for axon pathfinding and extension in the C. elegans nerve ring. Development. 1999;126(16):3679–3692. doi:10.1242/dev.126.16.3679.

Zallen JA, Yi BA, Bargmann CI. The conserved immunoglobulin superfamily member SAX-3/Robo directs multiple aspects of axon guidance in C. elegans. Cell. 1998;92(2):217–227. doi:10.1016/S0092-8674(00)80916-2.

Communicating editor: J. Ward